Formylmethanofuran: tetrahydromethanopterin formyltransferase from *Methanopyrus kandleri* — new insights into salt-dependence and thermostability

U Ermler[1]*, MC Merckel[1], RK Thauer[2] and S Shima[2]

Background: Formylmethanofuran: tetrahydromethanopterin formyltransferase (Ftr) from the methanogenic Archaeon *Methanopyrus kandleri* (optimum growth temperature 98°C) is a hyperthermophilic enzyme that is absolutely dependent on the presence of lyotropic salts for activity and thermostability. The enzyme is involved in the pathway of carbon dioxide reduction to methane and catalyzes the transfer of formyl from formylmethanofuran to tetrahydromethanopterin.

Results: The crystal structure of Ftr, determined to a resolution of 1.73 Å, reveals a homotetramer composed essentially of two dimers. Each subunit is subdivided into two tightly associated lobes both consisting of a predominantly antiparallel β sheet flanked by α helices forming an α/β sandwich structure. The approximate location of the active site was detected in a region close to the dimer interface.

Conclusions: The adaptation of Ftr against high lyotropic salt concentrations is structurally reflected by a large number of negatively charged residues and their high local concentration on the surface of the protein. The salt-dependent thermostability of Ftr might be explained on a molecular basis by ionic interactions at the protein surface, involving both protein and inorganic salt ions, and the mainly hydrophobic interactions between the subunits and within the core.

Addresses: [1]Max-Planck-Institut für Biophysik, Heinrich-Hoffmann-Straße 7, 60528 Frankfurt, Germany and [2]Max-Planck-Institut für terrestrische Mikrobiologie and Laboratorium für Mikrobiologie, Philipps-Universität, Karl-von-Frisch-Straße, 35043 Marburg, Germany.

*Corresponding author.
E-mail: ermler@max.mpibp.uni-frankfurt.de

Key words: crystal structure, formyltransferase, halophilic enzymes, hyperthermophilic enzymes, methanogenic Archaea, *Methanopyrus kandleri*

Received: 1 January 1997
Revisions requested: 29 January 1997
Revisions received: 1 April 1997
Accepted: 1 April 1997

Structure 15 May 1997, 5:635–646
http://biomednet.com/elecref/0969212600500635

Introduction

Formylmethanofuran: tetrahydro-methanopterin formyltransferase (Ftr) from *Methanopyrus kandleri* (a hyperthermophilic Archaeon with an optimum growth temperature of 98°C) is a soluble enzyme composed of only one type of subunit with an apparent molecular mass of 35 kDa [1]. At low concentrations (< 0.1 M) of lyotropic salts (K_2HPO_4 or $(NH_4)_2SO_4$) the protein is present in a catalytically inactive, monomeric state and denatures rapidly at temperatures above 50°C. At high salt concentrations Ftr assembles into a homotetramer, is active and stable to nearly 130°C (SS, UE, H Fukada, K Takahashi and RKT, unpublished results). The gene encoding Ftr from *M. kandleri* has been cloned, sequenced and functionally overexpressed in *Escherichia coli* [2]. The enzyme, which is stable under oxic conditions, is devoid of a chromophoric prosthetic group. Ftr catalyzes the transfer of a formyl group from formylmethanofuran to tetrahydromethanopterin via a ternary complex type catalytic mechanism [1]. For comparison the primary structures of Ftr from *Methanosarcina barkeri* (optimum growth temperature 37°C) [3], *Methanobacterium thermoautotrophicum* (65°C) [4], *Methanothermus fervidus* (83°C) [5] and *Methanococcus jannashii* (85°C) [6] are available.

In *M. kandleri*, which grows on H_2 and CO_2 with the formation of methane, Ftr catalyzes a reaction involved in methanogenesis [7]. This is a unique biological pathway involving novel coenzymes and enzymes [8,9]. The structures of all the coenzymes have previously been elucidated [10] but the study presented here reports the first structural analysis of an enyzme of the methanogenic pathway.

The crystal structures of only four enzymes from hyperthermophilic organisms (growth temperature optimum above 80°C) have, until now, been published: aldehyde ferredoxin oxidoreductase from *Pyrococcus furiosus* (100°C) at 2.3 Å [11]; glutamate dehydrogenase from *P. furiosus* at 2.2 Å [12]; glyceraldehyde-3-phosphate dehydrogenase from *Thermotoga maritima* (80°C) at 2.5 Å [13]; and indol-3-glycerol phosphate synthase from *Sulfolobus solfataricus* (87°C) at 2.0 Å resolution [14]. We report here the crystal structure of Ftr from *M. kandleri* at 1.73 Å resolution. Ftr differs from the other four enzymes studied in not only being adapted to high temperatures but also to high concentrations (> 1 M) of lyotropic salts present in the methanogenic Archaeon [15–17]. The tolerance of Ftr to lyotropic salts, like K_2HPO_4 or $(NH_4)_2SO_4$, provides a close relationship to halophilic proteins although those are optimally adapted to high salt concentrations of NaCl, KCl or $MgCl_2$. The observed high salt adaptation and salt-dependent thermostability are interpretated on the basis of the crystal structure.

Results

Structure determination

The crystal form P of Ftr was grown at a salt concentration of 0.3 M $(NH_4)_2SO_4$ [18], where the protein in solution is present partly in the monomeric form (see Introduction). However, the biologically relevant tetrameric form was observed in the crystal structure. Obviously crystallization in 0.3 M $(NH_4)_2SO_4$, pH 7.0 at high polyethylene glycol concentrations also favours oligomeric assembly.

The structure of Ftr in the tetrameric form has been determined by the multiple isomorphous replacement (MIR) method. After improving the initial map by solvent flattening, histogram matching and fourfold molecular averaging the polypeptide chain could be traced. The model has been refined to a conventional and free R factor of 19.2% and 24.3%, respectively, in the resolution range 1.73–10.0 Å. The model is composed of all 4×296 residues (8884 atoms) and 188, 150, 181, and 163 water molecules (present in subunits 1–4, respectively). An alternative conformation was only found for Cys58. The root mean square (rms) deviation of the polypeptide model from the ideal stereochemistry is 0.008 Å for bond lengths and 0.97° for bond angles. The average temperature factor for the protein is 22 Å^2. The quality of the final electron-density map is documented in Figure 1. There are no chain breaks. An alternative conformation was only found for Cys58. Poor electron density was observed for several charged solvent-exposed sidechains: Glu111, Glu133, Glu136, Glu232, Asp233, Glu238, Lys241 and Glu254. A structure obtained from a high salt crystal form (not available yet) could distinguish, whether the high temperature factors are a consequence of their solvent-exposed positions or of the low salt concentration. The average coordinate error was determined to be 0.11 Å, as obtained from the diffraction data precision indicator $\sigma_w(x)$ [19]. The Ramachandran plot [20] indicated that all non-glycine residues have favourable dihedral angles. The average per residue real-space correlation [21] between the model and the $2|F_o|-|F_c|$ electron density is 0.86; no residue has a value below 0.7.

An overlay of the four monomers in the asymmetric unit reveals a nearly identical backbone conformation reflected by a low overall rms deviation of 0.25 Å, using only the Cα atoms for superposition [21].

Monomer structure

A single subunit of Ftr has a size of 30 Å×40 Å×70 Å and can be subdivided into two tightly associated lobes with a small intermediate crevice (Fig. 2). Both the N- and the C-terminal ends of the polypeptide chain are located in the same lobe, which is therefore named the proximal lobe. The other lobe is consequently designated the distal lobe. The proximal lobe consists of residues 1–17 and 163–296, the distal lobe of residues 18–162. Both lobes belong to the class of α+β structures. The proximal lobe is basically built upon a four-stranded antiparallel β sheet enlarged by two small strands (1 and 2) close to the N-terminal end. The central β sheet is surrounded by two helices (D and E) at the front which pack against the distal lobe and the so-called insertion region, a region which is only loosely attached to the back of the central β sheet. This highly unusual insertion region extends between residues 198–241 and contains only two short, antiparallel oriented β strands (13 and 14) as secondary structure elements (Figs 2,3). The distal lobe comprises a seven-stranded β sheet composed of a four-stranded

Figure 1

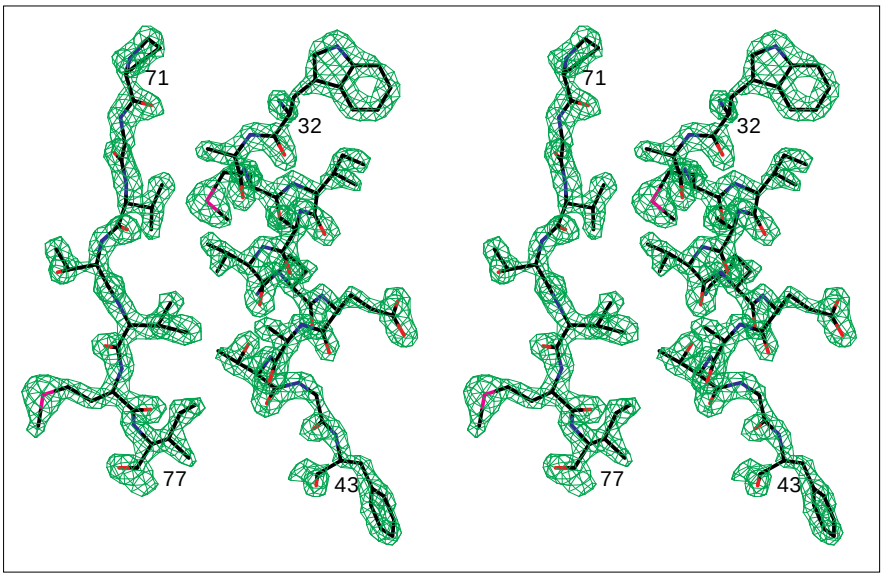

Representative section of the final $2F_o-F_c$ electron-density map at 1.73 Å resolution, contoured at a 2σ level. The region portrays a portion of β strand 5 and helix A of the distal lobe (see Fig. 2).

Figure 2

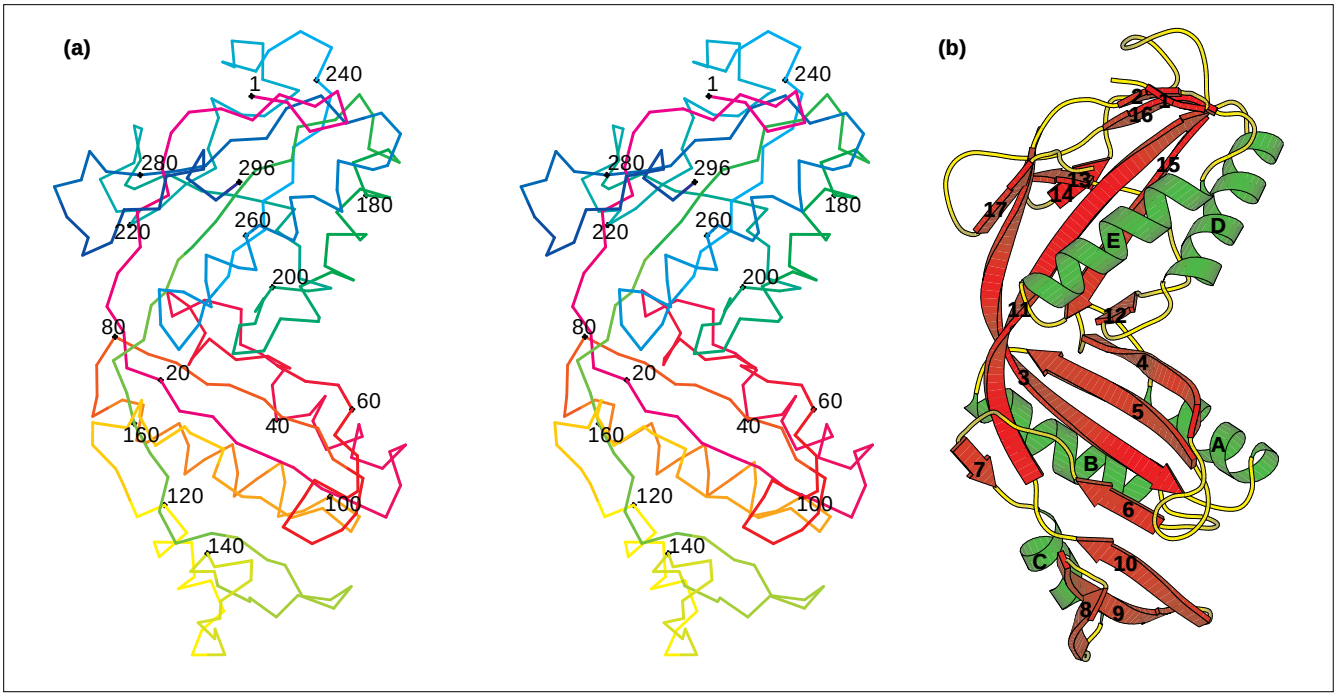

Structure of the Ftr monomer from *M. kandleri*. **(a)** 'Paint ramp' coloured stereoview of a Cα trace of Ftr labelled at every twentieth residue. (Figure generated with the program O [21].) **(b)** Ribbon diagram of Ftr showing the secondary structure elements. β Strands are shown as red arrows, α helices as green spirals and loops are in yellow. (The figure was drawn with the program MOLSCRIPT [53] and the secondary structure elements were calculated with the program DSSP [54].)

antiparallel β sheet combined with a β meander motif consisting of a three-stranded antiparallel β sheet. The whole β sheet is flanked by three α helices (A, B and C) on its backside and partly by the proximal lobe on its frontside (Fig. 2).

The extended and highly twisted β strands 3 and 11 belong to both lobes and serve as a covalent linker between them. They belong to the central β sheet at their C-terminal ends, form a common sheet in the center of the strands and each of them is joined with strands 7 and 17, respectively, at their N-terminal ends (Fig. 2). In addition to the described covalent junction, the two lobes are firmly tied by several noncovalent interactions either directly or mediated by bound water molecules. Consequently, the monomer can be considered as one entity. Arg22 plays a central role in the noncovalent connection of the lobes, in particular by forming two ion pairs to Asp57 and Glu194.

Both lobes contain extended hydrophobic core regions, each consisting of about 20 nonpolar sidechains. In the proximal lobe the hydrophobic cluster is located between the β strands 11, 12, 15 and 16 and the flanking α helices, D and E. Phe169 sits in the centre of the cluster and is in van der Waals contact with eight aliphatic residues, six of which are isoleucines. A preference for isoleucines was also described for a thermostable glutamate dehydrogenase [12]. The hydrophobic core in the distal lobe is formed by residues of the β strands 3, 5, 6, 9 and 10 and by α helices A, B and C.

Tetramer structure

Overall quaternary structure

Light scattering experiments in solution (SS, UE, H Fukada, K Takahashi and RKT, unpublished results) have shown that Ftr is present in the tetrameric state under physiological conditions. The packing in the crystals clearly supports Ftr as a homotetramer with dimensions of approximately 60 Å×75 Å×80 Å (Fig. 4). The tetramer has *222* symmetry and each monomer contacts all three symmetry-related partners. The monomers have been numbered 1, 2, 3 and 4 and the amino acids of the subunits were indexed with a superscript of the corresponding subunit to describe the intersubunit interactions.

A channel with a length of ~27 Å runs through the entire molecule parallel to the twofold axis relating subunits 1 and 4, or equivalently subunits 2 and 3 (Fig. 4). In the centre of the tetramer the channel becomes more voluminous and forms a cavity of ~12 Å in diameter. The entrance of the channel, formed by the crevices of subunits 1 and 4

Figure 3

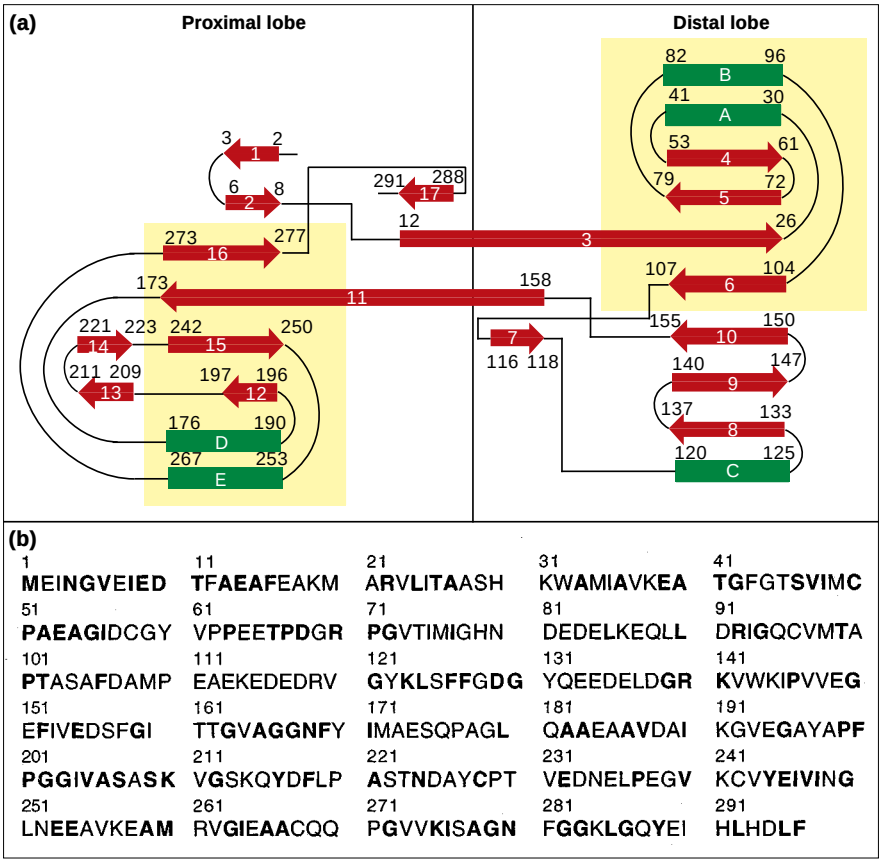

Primary and secondary structure assignment of Ftr from *M. kandleri.* **(a)** Topology diagram of Ftr; β strands are in red and α helices in green. The positions of the amino acid residues at each end of the structural elements are labelled. The core region of both lobes is indicated by a background of yellow shading. **(b)** The amino acid sequence of Ftr from *M. kandleri*; letters in bold indicate amino acids conserved in all five formyltransferases investigated [3].

Figure 4

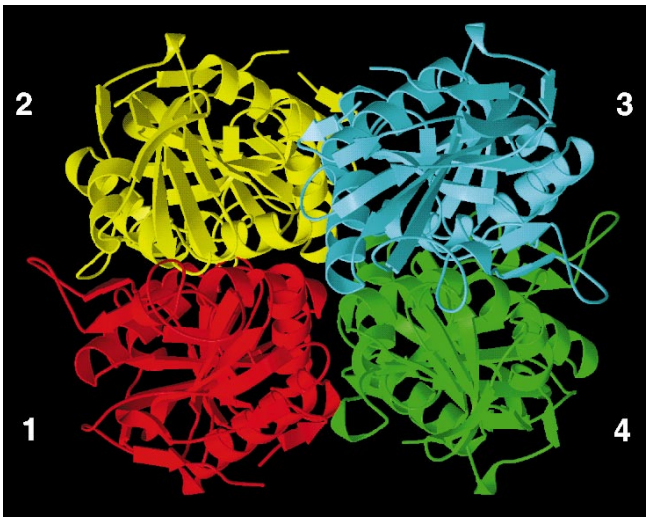

Ribbon diagram of the tetrameric state of Ftr. Subunits 1, 2, 3 and 4 are drawn in red, yellow, blue and green, respectively. A particularly extended contact occurs between subunits 1 and 2 (and the equivalent subunits 3 and 4). (The figure was produced with the programs MOLSCRIPT [53] and Raster3D [55].)

on one side of the tetramer and of subunits 2 and 3 on the other side, has a minimal diameter of ~6Å. The channel and the cavity are almost completely filled by firmly bound water molecules.

Subunit interfaces

The surface buried by tetramer assembly has been determined to be ~4000 Å^2 per monomer [22], which means that 30% of the solvent-exposed area of the monomer is buried after oligomerization. The overall interface area is 66% hydrophobic, 18% neutral polar and 16% charged. This compares well to interface hydropathy values of 65% nonpolar, 22% polar, and 13% charged derived from a survey of 23 oligomeric proteins [23,24]. However, the three intersubunit interfaces in Ftr differ markedly with regard to the size of the buried area, the contacting secondary structure segments, and the mode of interacting forces. Therefore, they have to be explored individually.

Subunits 1 and 2 (and the equivalent subunits 3 and 4) bury a large surface area of 2900 Å^2 which accounts for nearly 75% of the buried area of the tetramer. Consequently, the tetrameric state of Ftr can be described more correctly as a dimer of dimers. The buried area is

Figure 5

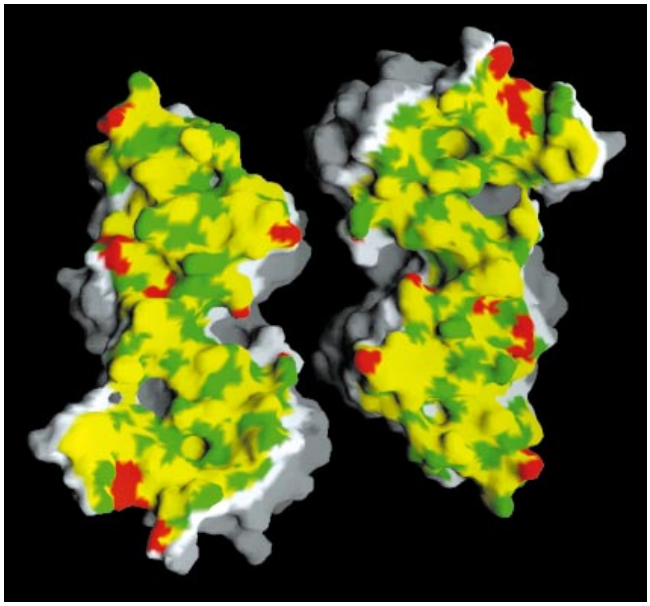

The contact area between subunits 1 and 2 (3 and 4), separated and rotated 90° towards the viewer. Hydrophobic, neutral polar and charged residues of the interface are coloured in yellow, green and red, respectively. Surface vertices 4–6 Å away from the interface are coloured in white and those beyond 6 Å are in grey. (Figure prepared with the program GRASP [41].)

composed of about 68% nonpolar, 21% neutral polar and 11% charged atoms.

The assembly of the monomers leads to one contact point which reaches from the insertion region via the core of both lobes to the β meander. The monomers are mutually oriented such that three loop segments of the β meander and the loop following helix B of subunit 2 pack against the insertion region of subunit 1, and vice versa on the opposite side of the interface (Fig. 5). The interface contact is dominated by hydrophobic interactions but specific polar interactions (listed in Table 1) also play an important role. For instance, an ion pair cluster is formed at the protein surface between residues Lys210[1], Lys214[1], Asp225[1] and Asp129[2] protruding from the loop connecting helix B and β strand 6. Asp129[2] also anchors the exposed insertion region via three hydrogen bonds to the sidechain of Ser213[1] and the peptide amine group of Lys214[1] and Gln215[1]. A hydrophobic patch consisting of Trp32[1], Ile35[1], Pro101[1], Leu180[2], Ile204[2] and Tyr244[2] weaves together distinct regions of the proximal and distal lobes by van der Waals interactions and connects the hydrophobic cores of the two subunits.

At the centre of the interface helices A and B pack against the loops following helices A and D, and vice versa. This contact is characterized by a hydrophobic cluster composed

Table 1

Intersubunit hydrogen bonds.

Donor		Acceptor	Distance* (Å)
Monomer 1	→	Monomer 2	
Lys31 Nζ		Glu184 Oε2	2.7
Glu31 Oε1		Phe43 N	3.3
Glu39 Oε1		Gly44 N	3.0
Glu39 O		Phe43 N	3.0
Thr45 Oγ1		Gln95 O	2.9
Met49 N		Gln95 Nε2	3.1
Gln95 Nε2		Ser46 Oγ	3.2
Gln95 Nε2		Ser46 O	3.1
Thr99 O		Ala206 N	2.9
Phe127 O		Thr223 N	2.9
Asp129 Oδ1		Ser213 Oγ	2.5
Asp129 Oδ1		Lys214 N	3.1
Asp129 Oδ1		Gln215 N	3.0
Asp129 Oδ2		Lys210 Nζ	2.8
Asp129 Oδ2		Lys214 N	3.0
Gln132 Nε2		Tyr216 OH	2.9
Pro146 O		Thr223 Oγ1	2.7
Val148 O		Val243 N	2.9
Glu149 N		Ala206 O	3.2
Glu149 Oε1		Tyr244 OH	2.8
Gly150 O		Thr230 Oγ1	3.2
Monomer 1	→	Monomer 3	
Gln176 Oε1		Gln181 Nε2	2.9
Gln176 Nε2		Gln181 Oε1	3.0
Monomer 1	→	Monomer 4	
His30 N		Asp188 Oδ2	2.9
Tyr60 OH		Asp188 O	2.5
Glu64 Oε2		Arg261 NH1	2.9
Glu64 Oε2		Arg261 NH2	3.0

*The maximum distance for hydrogen bonds was 3.3 Å.

of the sidechains of Phe43[1], Pro51[1], Arg92[1], Phe43[2], Pro51[2] and Arg92[2]. The guanidinium group of Arg92[1(2)] and the aromatic sidechain of Phe43[2(1)] provide an amino-aromatic interaction frequently found in proteins [25].

The interface area between subunits 1 and 3 (2 and 4) is very small (275 Å^2 per monomer) and represents only 2% of the entire surface of the monomer. There is only one point of contact formed between helix D, the following loop and the equivalent segments of the symmetry-related partner. A small hydrophobic region between Ala178[1] and Pro177[1] and their symmetry mates exists in the centre of the interface flanked by polar interactions at the edges (Table 1).

The buried area between subunits 1 and 4 (2 and 3) has a size of ~750 Å^2, which is equivalent to 6% of the entire surface of the monomer. This contact is characterized as relatively polar compared to the average chemical composition of interfaces [24]. Helices D and E of the proximal lobe pack against the loop between β strands 4 and 5 of

Figure 6

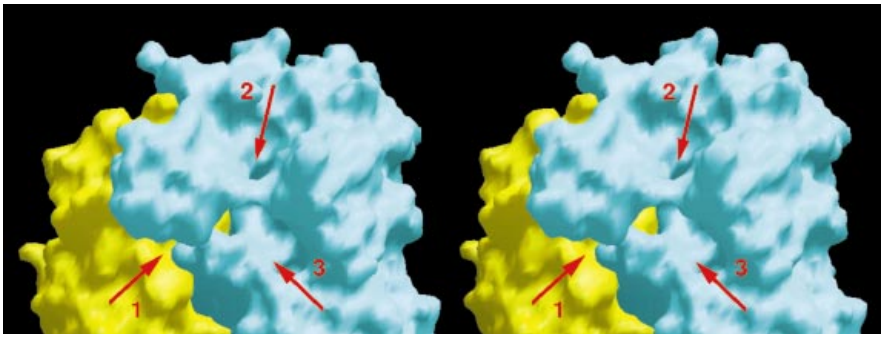

Stereoview of the Ftr protein surface indicating three clefts as potential substrate-binding sites linked in the interior of the protein. The active site is likely to be located in the insertion region close to the neighbouring subunit. The entrances of the pockets are indicated by red arrows and the two subunits are displayed in blue and yellow. (Figure produced with the program GRASP [41].)

the distal lobe, and vice versa, forming two points of contact. Of the eight intersubunit hydrogen bonds (Table 1), the interaction between the carbonyl group of Asp188[1] and the peptide nitrogen of His30[4] is particularly noteworthy, because the negatively charged aspartate stabilizes the N-terminal side of helix A. The polar nature of this packing interaction is further reinforced by a series of firmly bound water molecules.

Surface of the tetramer

The chemical composition of the accessible surface of the tetramer is 50% nonpolar, 22% neutral polar and 28% charged, whereas in typical oligomeric proteins the ratio of the mean values is 57%, 22% and 21%, respectively [24]. The fraction of neutral polar residues remains constant whereas the relative proportion of charged residues is significantly increased at the expense of nonpolar residues. The charged surface residues are composed of 46% glutamate, 21% aspartate, 7% arginine, 21% lysine and 5% histidine, which results in a dominance of glutamates over aspartates, lysines over arginines and negatively charged over positively charged residues.

Discussion

Ftr is composed of α/β sandwich motifs

The structure analysis reveals a common structural pattern of the core fold in both lobes, consisting of an antiparallel four-stranded β sheet flanked by two α helices. The schematic topology diagram shows an identical connectivity of the secondary structure elements in the two cores, emphasized by a yellow background in Figure 3a. In addition, an overlay of the two core regions indicates a high agreement in the relative positions and orientations of the four strands and the two helices, reflected by an rms deviation of 1.4 Å using 71 of 87 Cα atoms (82%) for superposition within the program GA_FIT [26]. However, some regions, in particular the loop regions, adopt markedly different conformations. Most noticeably, the insertion region of the proximal lobe contains ~40 residues whereas the equivalent loop in the distal lobe comprises only eight residues. Although no significant sequence homology could be detected between the core of the two lobes, their similarity suggests a common ancestor from which the basic fold of Ftr was built up by gene duplication.

The basic architecture of both lobes characterizes Ftr as a member of the large α+β structure family forming two α/β sandwiches. As observed for other α/β sandwiches, Ftr packs its hydrophobic core between the layer of β strands and α helices and uses hydrophobic surfaces or loops to bind to other proteins. The core fold of both lobes can be classified as double intertwined split βαβ folds [27], which represents a subgroup of α/β sandwiches found in several functionally distinct proteins. The smallest structural deviations were identified for related segments of malonyl-CoA:acyl carrier protein transacylase (MLA) [28], D-3-phosphoglycerate dehydrogenase (PSD) [29], and the signal transducing protein P_{II} (PIL) [30] (using the Z score of the program DALI [31]). The rms deviation between equivalent residues of Ftr and MLA (PSD, PIL) was 1.4 Å (1.6 Å, 1.7 Å), where 53 (55, 58) from 68 (74, 87) residues were selected for use in the calculation. Another α/β sandwich motif found in Ftr is the αβββ (or βββα) meander fold which is fused to the double intertwined split βαβ fold forming the distal lobe [27]. In summary, despite a unique overall architecture of Ftr, the secondary structure topology and the tertiary structure of smaller building blocks are already well known.

The enzymatic reaction

Ftr catalyzes the transfer of formyl from formylmethanofuran to tetrahydromethanopterin within the methanogenic pathway. Unfortunately, soaking and co-crystallisation experiments of Ftr with these large substrates were unsuccessful, so that a detailed enzymatic mechanism cannot be postulated. However, analysis of the surface profile revealed three sufficiently large, interconnected clefts (Fig. 6) which might be used as binding sites for the substrates. Within subunit 1, two pockets are formed by residues of the insertion and core regions of the proximal lobe (see Fig. 6; arrows 2 and 3). The third pocket is built up at the interface between the insertion region of subunit

1 and helices B and C of subunit 2 (see Fig. 6; arrow 1). The arrangement of the pockets suggests that the active site is located in the insertion region close to the neighbouring subunit. It is an open question as to whether the neighbouring subunit is involved in substrate binding or only in keeping the insertion region in a certain conformation. The proposed location of the active site involving two subunits is supported by the fact that the monomeric form of the enzyme, present at low lyotropic salt concentrations (< 0.5 M) [1], is inactive. Moreover, the residues of segments 45–48, 199–212 and 277–281 (of subunit 1) and of segments 98–99 and 126–127 (of subunit 2), which are probably involved in forming the clefts, are highly conserved in the formyltransferases with known primary structure [3] (Fig. 3b).

Interestingly, we find electron density in the potential active-site region which cannot be interpreted as solvent. However, the occupancy of this ligand is low and it cannot be a methanogenic coenzyme as Ftr was expressed in *E. coli* [2].

Adaptation to high concentrations of lyotropic salts

High intracellular lyotropic salt concentrations have forced the proteins of *M. kandleri* [16] to develop special adaptation mechanisms to avoid aggregation, precipitation or even unfolding. A structural analysis of Ftr revealed two features that can be correlated with the unusually high solubility of this protein under high salt conditions.

Firstly, the hydrophobic proportion of the surface area of the protein is decreased from 57%, as observed in a normal mesophilic protein, to 50% for Ftr. This effect should reduce the tendency for aggregation.

The second, more striking structural feature of Ftr is the excess of negative charges at the protein surface (48 acidic residues and the C-terminal carboxyl group as compared to 24 basic residues). The molecular mechanism by which the dominance of negative charges (illustrated in Fig. 7 as negative surface potential) increase solubility at high salt concentrations is unknown. An important factor might be the property of acidic residues to form strong and multiple hydrogen bonds to water molecules, which enables them to compete with inorganic cations or water molecules. Glutamate has a higher capacity for binding water molecules than all other residues [32], which could explain its preference over aspartate (33 glutamate versus 15 aspartate) in Ftr. The enhanced capacity of acidic residues for binding water molecules could not be confirmed in the crystal structure, perhaps due to the low salt concentration used in the crystallization conditions.

Furthermore, the acidic residues are not evenly distributed but clustered at the surface, most strikingly in the segments from 81–88 (six acidic and one basic residue), 111–119 (six acidic and two basic) and 133–141 (five acidic and two basic) (Fig. 8). A local accumulation of acidic residues might enhance the capability of the protein to bind water molecules or hydrated salt cations. Despite their local accumulation neighbouring carboxylate groups are mostly positioned more than 4 Å apart, this is helpful in avoiding protonation. One of the exceptions is the distance of 3.2 Å observed between Asp116 and Asp118, however, the adjacent Lys86 acts to neutralize the proximity of the two negative charges (see Fig. 8).

The basic structural principles for high salt adaptation in Ftr, namely the excess of negative charges and their high

Figure 7

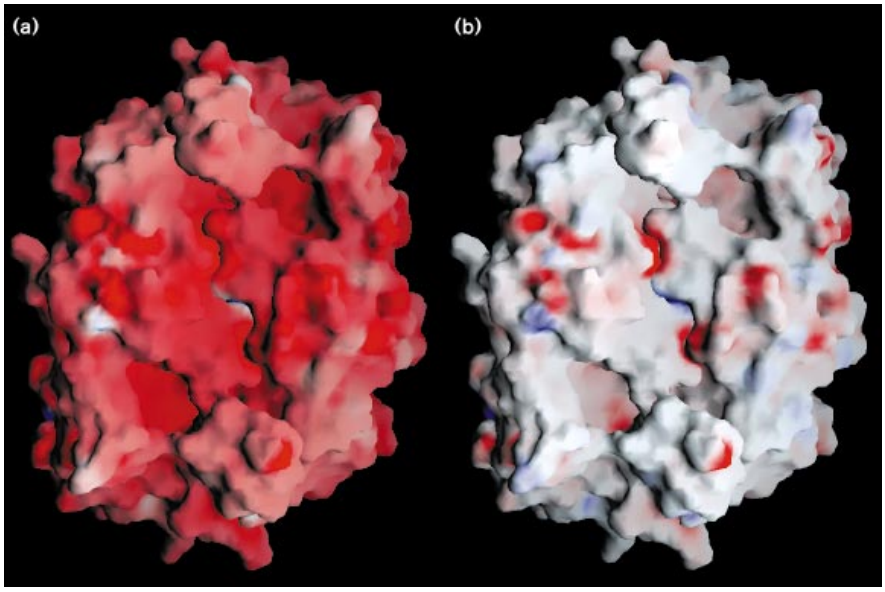

The electrostatic properties of the Ftr monomer. The molecular surface is colour-coded according to the electrostatic potential: the extreme ranges of red and blue represent potentials of $-40\,k_BT$ and $40\,k_BT$, respectively (where k_B = Boltzmann constant and T = temperature). **(a)** The electrostatic potential without salt, demonstrating the excess of negative charges on the protein surface. **(b)** The electrostatic potential at a salt concentration of 1.5 M, where the surface potential is nearly neutral. (Figure generated using the program GRASP [41].)

Figure 8

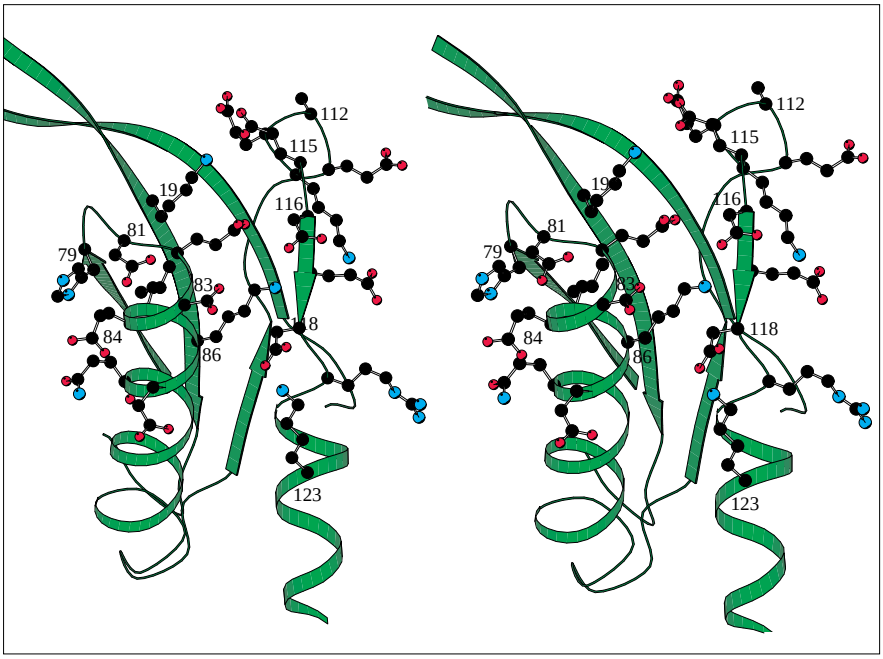

Stereoview showing a surface region of Ftr where basic and, in particular, acidic residues are clustered in the segments 81–88 and 111–119. Lys86 is surrounded by four acidic residues, Glu82, Asp83, Asp116 and Asp118. Atoms are shown in standard colours and labelled. (Figure generated using the program MOLSCRIPT [53].)

local concentrations, are in accordance with other studies [33]. In particular, these observations are in line with studies of the recently established structures of malate dehydrogenase [34] and 2Fe–2S ferredoxin [35] from the extremely halophilic Archaeon *Haloarcula marismortui*.

Thermophilic adaptation

As known from other studies the strategies for protein thermostability are highly diverse and rather complex [36]. Several factors are presumably highly interconnected and cannot be easily reduced to individual structural features. The discussion is further hampered as no crystal structure of a mesophilic counterpart of Ftr is available. Therefore, we will focus only on three determinants for thermostability which are comparable to those derived from structures of other thermostable proteins or which can be related to other experimental data. These three structural factors are the oligomerization of the protein, ionic interactions at the protein surface and multiple connections between different segments of the structure.

Oligomerization

Strong experimental evidence for the extraordinary importance of tetramer formation for thermostability is provided by calorimetric measurements, which exploit the useful property of Ftr being stable in its monomeric and tetrameric state. The melting temperature for the monomer at low lyotropic salt concentrations was approximately 50°C whereas the melting temperature for the tetramer at high lyotropic salt concentrations was nearly 130°C (SS, UE, H Fukada, K Takahashi and RKT, unpublished results). Presumably, the major stabilizing contribution is due to the extended dimer interface the surface of which is illustrated as a colour-coded hydropathy plot in Figure 5.

The predominantly nonpolar character of the interface in Ftr contributes to hydrophobic interactions which probably have an important stabilizing role, as found for glyceraldehyde-3-phosphate dehydrogenase from *T. maritima* [13]. The shielding of hydrophobic residues at the subunit interface results in a decrease of the enthalpic term, but also in an increase of the entropic term, by disordering the water molecules located around apolar groups prior to tetramer formation.

Charged residues are predominantly found at the edges of the interface (Fig. 5) and are thus solvent-exposed. The only exception is Arg92 that forms an intersubunit amino–aromatic interaction to Phe43 and three hydrogen bonds to the peptide carbonyl oxygens of Ala40, Gly42 and Phe43.

The apparent importance of oligomeric interactions was also reported for an inorganic pyrophosphatase from *Thermus thermophilus* [37], triosephosphate isomerase from *Bacillus stearothermophilus* [38] and malate dehydrogenase from *Thermus flavus* [39].

Ionic interactions at the surface

The presence of ion-pair networks is emphasized in several reports as a major factor for thermostability. For Ftr, the number of ion pairs per residue was calculated as

0.07, which is higher than the average value of 0.04 for mesophilic proteins [40]. However, this value is significantly lower than that for some other hyperthermostable proteins, such as glutamate dehydrogenase [12] and aldehyde ferredoxin oxidoreductase [11]. In Ftr, the ion pairs are predominantly located at the protein surface (Fig. 8). From 77 charged residues only 6% of the sidechains have a solvent accessibility below 10%. The ion pairs are mostly concentrated in larger clusters reflected in the formation of two quadruple and four triple ion-pair networks. The majority of the multiple ion pairs are constructed so as to join different secondary structure elements on the protein surface. For example in the distal lobe, helix B of the core region is linked to helix C of the β meander region via β strand 7 by forming ion interactions between Lys86 and Asp116, Lys86 and Asp118 and between Asp118 and Lys123 (Fig. 8).

The excess negative charge on the surface of the protein is probably compensated for by hydrated salt cations. Potentially bound salt cations (NH_4^+) cannot be distinguished from water molecules in the electron density, but their influence upon the surface potential can be simulated within the program GRASP [41]. At 1.5 M salt concentration the overall distribution of charges on the surface is balanced as visualized in Figure 7.

Multiple connections

A rough indicator of multiple and optimized interactions within the polypeptide chain is the rigidity of a structure; the rigidity is approximately described in terms of the isotropic crystallographic temperature factor. It is striking that all backbone atoms of Ftr have a relatively low temperature factor and a clearly defined electron density. The observed high structural rigidity can be correlated with several structural features.

The insertion region, only loosely anchored to the core, interacts extensively with the β meander region of the neighbouring subunit (see above) which 'freezes' both parts (Fig. 5). The two lobes of the subunits are tightly associated by multiple interactions. All of the loop regions that join secondary structure elements are multiply linked to adjacent polypeptide regions of the same or neighbouring subunits, mainly by hydrogen-bond interactions.

The N- and C-terminal residues, Met1 and Phe296, are tightly connected to each other and to the protein matrix. The sidechains of Met1 and Phe296 form, together with Ile3, Ile8, Ile264 and Leu295, a hydrophobic cluster which is linked to the hydrophobic core of the proximal lobe. These interactions, together with some additional polar interactions, lead to an increased rigidity of the region reflected by the low temperature factors of Met1 (18.4 $Å^2$) and Phe296 (24.7 $Å^2$). In indole-3-glycerol phosphate dehydrogenase from *S. solfataricus* [14] the N- and C-terminal residues are not mutually linked but are also strongly tied to the polypeptide framework.

In summary, the most striking structural features of thermophilic adaptation at high salt conditions appear to be the presence of ion-pair networks, composed of charged sidechains and inorganic salt cations at the protein surface, and the formation of extended hydrophobic regions within the core and between subunits. Increasing lyotropic salt concentrations enhance both ionic and hydrophobic interactions due to an increasing number of inorganic cations at the negatively charged protein surface and the salting-out effect, respectively, thus providing a molecular interpretation of the salt-dependent thermostability of Ftr. In light of these results one might speculate as to whether certain organisms utilize high intracellular salt concentrations as a tool to reach stability at extreme temperatures.

The described mechanism of salt-dependent thermoadaptation has not forced the protein to develop simultaneously a strategy for adaptation against high lyotropic salt concentrations. The excess of negatively charged residues on the protein surface increases the number of ionic interactions on the one hand and keeps the protein in solution on the other. Therefore, the structural determinants for high salt adaptation and thermostability are highly interconnected in Ftr and support each other optimally.

Biological implications

A group of strictly anaerobic Archaea utilize the methanogenic pathway for energy generation. The reduction of carbon dioxide to methane involves several novel enzymes and coenzymes. One of these enzymes is formylmethanofuran: tetrahydromethanopterin formyltransferase (Ftr), which catalyzes the transfer of formyl from formylmethanopterin to tetrahydromethanopterin. The structure reported here, of Ftr from *Methanopyrus kandleri*, represents the first three-dimensional structure to be determined for an enzyme of a hyperthermophilic methanogenic Archaeon and of an enzyme of the methanogenic pathway. At physiological high salt concentrations, Ftr is present as a homotetramer with 296 residues per subunit. Each subunit can be subdivided into two lobes both folded into an **α/β** sandwich arrangement. The active site of the enzyme is presumably located close to the interface between the two subunits where three pronounced clefts at the protein surface merge in the interior of the protein.

Ftr can withstand extreme environmental conditions: it maintains its native conformation up to a temperature of 130°C in the presence of high lyotropic salt concentrations. This property requires a unique salt-dependent thermoadaptation mechanism and a mechanism to keep the protein in solution under high salt conditions. The

crystal structure of Ftr at 1.73 Å reveals several structural features with potential implications for thermostability and high salt adaptation. The basic strategy for adaptation to high salt concentrations appears to be a high number of negatively charged residues and their local accumulation on the surface of the protein. These observations agree well with those of previous results from halophilic proteins. Two prominent structural features for thermoadaptation are evident: the extended contact area between the subunits, and especially the high proportion of nonpolar residues involved; and ion-pair networks both within the protein and between acidic residues and inorganic cations. The ionic and the hydrophobic interactions increase with increasing lyotropic salt concentrations, which might explain the salt-dependent thermostability of Ftr on a molecular level.

Materials and methods

Crystallization and data collection

Ftr from *M. kandleri* was overexpressed in *E. coli*, purified to homogeneity and crystallized as described previously [2,18]. Three crystal forms (M, P and S) were obtained but only crystals of form P were used for structure determination. Crystallization was achieved in the presence of 22% polyethylene glycol 8000, 0.3 M $(NH_4)_2SO_4$ and 0.1 M Mops, pH 7 using the hanging-drop method. The bipyramidal crystals diffracted up to 1.7 Å resolution and belonged to the space group $I4_122$ with cell dimensions of 157.5 Å and 242.2 Å, compatible with one tetramer per asymmetic unit. Native data set 1 (Nat1) and all derivative data sets were collected in house on a R-AXIS II image-plate detector with CuK_α radiation from a Rigaku rotating-anode generator. Data processing and scaling were carried out with the program MOSFLM and the CCP4 package [42,43]. The quality of the reflection intensities are listed in Table 2. Native data set 2 (Nat2) was collected with synchrotron radiation ($\lambda = 1$ Å) at the Max-Planck-beamline at DESY (Deutsches Elektronensynchrotron, Hamburg) using a MAR-Research image-plate as detector. The resulting R_{sym} was 5.4% and the completeness 87.7% in the resolution range 1.73–10.0 Å (Table 2).

Phase determination

The structure of Ftr has been solved by the MIR method. Two heavy-atom derivatives yielded reasonable phasing parameters (summarized in Table 2). One site of the lead derivative could be localized in the difference Patterson map using SHELXS [44] for interpretation. The obtained heavy-atom positions were refined and SIR phases calculated with the program MLPHARE [45]. Further heavy-atom sites were detected by difference Fourier techniques. Final phasing performed with one lead and one mercury derivative lead to a figure of merit of 0.38, between 10–3.2 Å resolution. The resulting MIR electron-density map could be dramatically improved by the solvent flattening (solvent content 60%) and the histogram matching option of DM [46] resulting in an R_{free} of 32.3% from 10–3.2 Å resolution. Subsequent fourfold molecular averaging with phase extension up to 2.8 Å was carried out using RAVE [47]. After 'skeletonization' of the electron density and separation of a single subunit with the programs MAPMAN [48] and O [21] a molecular mask of this subunit was generated with MAMA [47]. The noncrystallographic symmetry (NCS) operators were calculated from four heavy-atom sites per subunit within O and improved with the program IMP [47].

Model building and refinement

The solvent flattened and fourfold averaged electron-density maps of 3.2 Å and 2.8 Å resolution were of sufficient quality to build in a Cα trace with the 'Baton' option of O [21]. Finally, 282 of 296 amino acids could be incorporated into the electron density. The major problems during model building were to separate closely attached parts of different subunits and to fit the sequence into the electron density, as the N- and C-terminal ends are in van der Waals contact to each other and not easily detectable. The refinement was performed within X-PLOR [49] using the force field parameters developed by Engh and Huber [50]. During the first molecular dynamic minimization using the slow-cooling protocol (3000–300K) and a subsequent positional and temperature factor refinement the R factor and the R_{free} dropped to 24.3% and 30.0%, respectively, in the resolution range 10–2.5 Å. Afterwards the missing residues between 214 and 227 were visible in the $2F_o–F_c$ map. The second and following rounds of refinement utilized all data from 10.0–1.73 Å resolution. In the first rounds, equivalent atoms of the four subunits related by fourfold NCS symmetry were treated as restrained, in later stages the NCS restraints were omitted. Water molecules were built in when the $2F_o–F_c$ and the $F_o–F_c$ electron-density map were higher than 1σ and 3σ, respectively. Moreover, the map peak had to be roughly spherical and lie within 3.3 Å from a hydrogen-bond donor/acceptor. Water molecules with temperature factors greater than 50 $Å^2$ were removed from the model. After seven rounds of alternate automatic refinement and manual inspection of the electron density the R factor converged.

Analysis of the structure

Model errors were assessed using PROCHECK [51], which verifies deviations of geometric parameters (from ideal values) and dihedral

Table 2

Data collection and phasing statistics.

Data set	Native 1	Native 2	Hg*	Pb*
Resolution (Å)	2.7	1.73	3.5	3.2
R_{sym} (%)†	7.0	5.4	13.9	8.9
Completeness (%)	87.6	87.8	67.0	90.3
Multiplicity	2.8	3.0	1.8	2.9
R_{merge} (%)‡			31.4	13.5
No. of sites per monomer			2	2
R_{cullis} (%)§			0.79	0.64
Phasing power#			1.1	1.2

*Hg = mersalylic acid, 0.5 mM, 8 h and Pb = $(CH_3)_3$Pb acetate, 1 mM, 30 h; the reservoir solution was used for heavy-atom soaking experiments. †$R_{sym} = \Sigma_{hkl}\Sigma_i|I_i - <I>|/\Sigma <I>$, where I_i is the intensity of the i^{th} measurement per reflection hkl and $<I>$ is the average intensity for a reflection. ‡$R_{merge} = \Sigma_{hkl}||F_p| - |F_{ph}||/\Sigma_{hkl}|F_p|$, where $|F_P|$ and $|F_{PH}|$ are the structure-factor amplitudes for the native protein and the heavy-atom derivatives, respectively. §$R_{cullis} = \Sigma_{hkl}(|F_{PH}(obs)| - |F_{PH}(calc)|)/\Sigma_{hkl}(|F_{PH}(obs)| - |F_P(obs)|)$, summed over centric reflections only. #Phasing power = F(H)/E, the root mean square (rms) heavy atom structure-factor amplitudes divided by the lack of closure error.

angles (from allowed regions) for the mainchain and sidechain atoms. The fit of individual coordinates to the electron density was checked by calculating the real-space correlation [21] between them. Structural superposition was either performed with GA_FIT [26] or within O [21], where the least-squares fit algorithm of Kabsch [52] is implemented. Similarities between the fold of Ftr and that of other structurally characterized proteins were identified with the DALI WWW server [31]. Ionic interactions were designated as salt bridges or ion pairs when their distances were below 4.0 Å [40]. Accessible surface areas were calculated with NACCESS [22] and the classification of the area into hydrophobic, uncharged polar and charged was performed according to Miller *et al.* [23].

Accession numbers

Coordinates will be deposited in the Brookhaven Data Bank.

Acknowledgements

We thank Hartmut Michel for generous support, Daniela Vinzenz for technical assistance and the staff of the Max-Planck beamline at DESY for station alignment.

References

1. Breitung, J., Börner, G., Scholz, S., Linder, D., Stetter, K.O. & Thauer, R.K. (1992). Salt dependence, kinetic properties and catalytic mechanism of *N*-formylmethanofuran: tetrahydromethanopterin formyltransferase. *Eur. J. Biochem*. 210, 971–981.
2. Shima, S., Weiss, D.S. & Thauer, R.K. (1995). Formylmethanofuran:tetrahydromethanopterin formyltransferase (Ftr) from the hyperthermophilic *Methanopyrus kandleri*: cloning, sequencing and functional expression of the *ftr* gene and one-step purification of the enzyme overproduced in *Escherichia coli*. *Eur. J. Biochem.* 230, 906–913.
3. Kunow, J., Shima, S., Vorholt, J.A. & Thauer, R.K. (1996). Primary structure and properties of the formyltransferase from the mesophilic *Methanosarcina barkeri*: comparison with enzymes from thermophilic and hyperthermophilic methanogens. *Arch. Microbiol.* 165, 97–105.
4. DiMacro, A.A., Sment, K.A., Konisky, J. & Wolfe, R.S. (1990). The formylmethanofuran: tetrahydromethanopterin formyltransferase from *Methanobacterium thermoautotrophicum* ΔH. Nucleotide sequence and functional expression of the cloned gene. *J. Biol. Chem.* 265, 472–476.
5. Lehmacher, A. (1994). Cloning, sequencing and transcript analysis of the gene encoding formylmethanofuran:tetrahydromethanopterin formyltransferase from the hyperthermophilic *Methanothermus fervidus*. *Mol. Gen. Genet.* 242, 73–80.
6. Bult, C.J., *et al.*, & Venter, J.C. (1996). Complete genome sequence of the methanogenic Archaeon, *Methanococcus jannaschii*. *Science* 273, 1058–1073.
7. Rospert, S., *et al.*, & Stetter, K.O. (1991). Methyl-coenzyme M reductase and other enzymes involved in methanogenesis from CO_2 and H_2 in the extreme thermophile *Methanopyrus kandleri*. *Arch. Microbiol.* 156, 49–55.
8. Wolfe, R.S. (1991). My kind of biology. *Annu. Rev. Microbiol.* 45, 1–35.
9. Thauer, R.K. (1996). Biodiversity and unity in biochemistry. *Anatonie van Leewenhoek* 71, 21–32.
10. DiMarco, A.A., Bobik, T.A. & Wolfe, R.S. (1990). Unusual coenzymes of methanogenesis. *Annu. Rev. Biochem.* 59, 355–394.
11. Chan, M.K., Mukland, S., Kletzin, A., Adams, M.W.W. & Rees, D.C. (1995). Structure of a hyperthermophilic tungstopterin enzyme, aldehyde ferredoxin oxidoreductase. *Science* 267, 1463–1469.
12. Yip, K.S.P., *et al.*, & Rice, D.W. (1995). The structure of *Pyrococcus furiosus* glutamate dehydrogenase reveals a key role for ion-pair networks in maintaining enzyme stability at extreme temperatures. *Structure* 3, 1147–1158.
13. Korndörfer, I., Steipe, B., Huber, R., Tomschy, A. & Jaenicke, R. (1995). The crystal structure of holo-glyceraldehyde-3-phosphate dehydrogenase from the hyperthermophilic bacterium *Thermotoga maritima* at 2.5 Å resolution. *J. Mol. Biol.* 246, 511–521.
14. Hennig, M., Darimont, B., Sterner, R., Kirschner, K. & Jansonius, J.N. (1995). 2.0 Å structure of indole-3-glycerol phosphate synthase from the hyperthermophile *Sulfolobus solfataricus*: possible determinants of protein stability. *Structure* 3, 1295–1306.
15. Huber, R., Kurr, M., Jannasch, H.W. & Stetter, K.O. (1989). A novel group of abyssal methanogenic archaebacteria (*Methanopyrus*) growing at 110°C. *Nature* 342, 833–834.
16. Kurr, M., *et al.*, & Stetter, K.O. (1991). *Methanopyrus kandleri* , gen. and sp. nov. represents a novel group of hyperthermophilic methanogens, growing at 110°C. *Arch. Microbiol.* 156, 239–247.
17. Burggraf, S., Stetter, K.O., Rouviere, P. & Woese, C.R. (1991). *Methanopyrus kandleri*: an archaeal methanogen unrelated to all other known methanogens. *Systematic Appl. Microbiol.* 14, 346–351.
18. Shima, S., Thauer, R.K., Michel, H. & Ermler, U. (1996). Crystallization and preliminary X-ray diffraction studies of formylmethanofuran:tetrahydromethanopterin formyltransferase from *Methanopyrus kandleri*. *Proteins* 26, 118–120.
19. Cruickshank, D.W.J. (1996). Protein precision re-examined: Luzzati plots do not estimate final errors. In *Proceedings of the CCP4 Study Weekend*. (Dodson, E., Moore, M., Ralph, A. & Bailey, S., eds), pp.11–22. Daresbury Laboratory , Warrington, UK.
20. Ramachandran, G.N., Ramakrishnan, C. & Sasisekharan, V. (1963). Stereochemistry of polypeptide chain configuration. *J. Mol. Biol.* 7, 95–99.
21. Jones, T.A., Zou, J.Y., Cowan, S.W. & Kjeldgaard, M. (1991). Improved methods for building protein models in electron-density maps and the location of errors in these models. *Acta Cryst. A* 47, 110–119.
22. Hubbard, S.J., Campell, S.F. & Thornton, J.M. (1991). Molecular recognition. Conformational analysis of limited proteolytic sites and serine proteinase protein inhibitors. *J. Mol. Biol.* 220, 507–530.
23. Miller, S., Lesk, A.M., Janin, J. & Chothia, C. (1987). The accessible surface area and stability of oligomeric proteins. *Nature* 328, 834–836.
24. Janin, J., Miller, S. & Chothia, C.H. (1988). Surface, subunit interfaces and interior of oligomeric proteins. *J. Mol. Biol.* 204, 155–164.
25. Flocco, M.M. & Mombray, S.L. (1994). Planar stacking interactions of arginine and aromatic side chains in proteins. *J. Mol. Biol.* 235, 709–717.
26. May, A.C.W. & Johnson, M.S. (1994). Protein structure comparisons using a combination of a genetic algorithm, dynamic programming and least-squares minimization. *Protein Eng.* 7, 475–485.
27. Orengo, C.A. & Thornton, J.M. (1993). Alpha plus beta folds revisited: some favoured motifs. *Structure* 1, 105–120.
28. Serre, L., Verbree, E.C., Dauter, Z., Stuitje, A.R. & Derewenda, Z.S. (1995). The *Escherichia coli* malonyl-CoA: acyl carrier protein transacylase at 1.5-Å resolution. Crystal structure of a fatty acid synthase. *J. Biol. Chem.* 270, 12961–12964.
29. Schuller, D.J., Grant, G.A. & Banaszak, L.J. (1995). The allosteric ligand site in the cooperative enzyme phosphoglycerate dehydrogenase. *Nat. Struct. Biol.* 2, 69–76.
30. Cheah, E., Carr, P.D., Suffolk, P.M., Vasudevan, S.G., Dixon, N.E. & Ollis, D.L. (1994). Structure of the *Escherichia coli* signal transducing protein P_{II}. *Structure* 2, 981–990.
31. Holm, L. & Sander, C. (1993). Protein structure comparison by alignment of distance matrices. *J. Mol. Biol.* 233, 123–138.
32. Kuntz, I.D. (1971). Hydration of macromolecules IV. Polypeptide conformation in frozen solutions, *J. Am. Chem. Soc*. 93, 516–518.
33. Zaccai, G. & Eisenberg, H. (1990). Halophilic proteins and the influence of solvent on protein stabilization. *Trends Biochem. Sci.* 15, 333–337.
34. Dym, O., Mevarech, M. & Sussman, J.L. (1995). Structural features that stabilize halophilic malate dehydrogenase from an archaebacterium. *Science* 267, 1344–1346.
35. Frolow, F., Harel, M., Sussman, J.L., Mevarech, M. & Shoham, M. (1996). Insights into protein adaptation to a saturated salt environment from the crystal structure of a halophilic 2Fe–2S ferredoxin. *Nat. Struct. Biol.* 3, 452–458.
36. Jaenicke, R. (1996). Stability and folding of ultrastable proteins: eye lens crystallins and enzymes from thermophiles. *FASEB J.* 10, 84–92.
37. Salminen, T., Teplyakov, A., Kankare, J., Cooperman, B.S., Lahti, R. & Goldman, A. (1996). An unusual route to thermostability disclosed by the comparison of *Thermus thermophilus* and *Escherichia coli* inorganic pyrophosphatases. *Protein Sci.* 5, 1014–1025.
38. Delboni, L.F., *et al.*, & Hol, W.G.H. (1995). Crystal structure of recombinant triosephosphate isomerase from *Bacillus stearothermophilus.* An analysis of potential thermostability factors in six isomerases with known three-dimensional structures points to the importance of hydrophobic interactions. *Protein Sci.* 4, 2594–2604.
39. Kelly, C.A., Nishiyama, M., Ohnishi, Y., Beppu, T. & Birktoft, J.J. (1993). Determinants of protein thermostability observed in the 1.9 Å crystal structure of malate dehydrogenase from the thermophilic bacterium *Thermus flavus*. *Biochemistry* 32, 3913–3922.

40. Barlow, D.J. & Thornton, J.M. (1983). Ion-pairs in proteins. *J. Mol. Biol.* 168, 857–885.
41. Nicholls, A., Bharadwaj, R. & Honig, B. (1993). GRASP: graphical representation and analysis of surface properties. *Biophys. J.* 64, 166–170.
42. Leslie, A.G.W. (1992). Recent changes to the MOSFLM package for processing film and image plate data. *Joint CCP4 and ESR-EACBM Newsletter on Protein Crystallography* 26, 83–91.
43. Collaborative Computational Project, Number 4. (1994). The CCP4 suite: programs for protein crystallography. *Acta Cryst. D* 50, 760–763.
44. Sheldrick, G.H. (1991). Heavy atom location using SHELXS-90. In *Proceedings of the CCP4 Study Weekend.* (Wolf, W., Evans, P.R. & Leslie, A.G.W., eds), pp. 23–38, Daresbury Laboratory, Warrington, UK.
45. Otwinowsky, Z. (1991). Maximum likelihood refinement of heavy atom parameters. In *Proceedings of the CCP4 Study Weekend.* (Wolf, W., Evans, P.R. & Leslie, A.G.W., eds), pp. 80–86, Daresbury Laboratory, Warrington, UK.
46. Cowtan, K.D. (1994). 'DM': an automated procedure for phase improvement by density modification. In *Joint CCP4 and ESF-EACBM Newsletter on Protein Crystallography* 31, 83–91.
47. Kleywegt, G.A. & Jones, T.A. (1994). 'Halloween — masks and bones.' In *Proceedings of the CCP4 Study weekend*. (Bailey, S., Hubbard, R. & Waller, D., eds), pp. 59–66, Daresbury Laboratory, Warrington, UK.
48. Kleywegt, G.J. & Jones, T.A. (1996). xdlMAPMAN and xdlDATAMAN — programs for reformatting, analysis and manipulation of biomacromolecular electron-density maps and reflection data sets. *Acta Cryst. D* 52, 826–828.
49. Brünger, A.T. (1992). *X-PLOR Version 3.1: A System for X-ray Crystallography and NMR*. Yale University Press, New Haven, CT, USA.
50. Engh, R.A. & Huber, R. (1991). Accurate bond and angle parameters for X-ray protein structure refinement. *Acta Cryst. A* 47, 392–400.
51. Laskowski, R.A., MacArthur, M.W., Moss, D.S. & Thornton, J.M. (1993). PROCHECK: a program to check the stereochemical quality of protein structures. *J. Appl. Cryst.* 26, 283–291.
52. Kabsch, W. (1978). A discussion of the solution for the best rotation to relate two sets of vectors. *Acta Cryst. A* 34, 827–828.
53. Kraulis, P.J. (1991). MOLSCRIPT: a program to produce both detailed and schematic plots of protein structures. *J. Appl. Cryst.* 24, 946–950.
54. Kabsch, W. & Sander, C. (1983). Dictionary of protein secondary structures: pattern recognition of hydrogen-bonded and geometrical features. *Biopolymers* 22, 2577–2637.
55. Merrit, E.A. & Murphy, M.E.P. (1994). Raster3D version 2.0. A program for photorealistic molecular graphics. *Acta Cryst. D* 50, 869–873.